



# Kent Academic Repository

Liu, Xuekang, Sanz-Izquierdo, Benito, Gao, Steven, Zhang, Haiwei, Hu, Wei and Yang, Xue-Xia (2023) *Wideband Dual-Polarized Antenna with High Selectivity for 5G Sub-6GHz Base Station Applications*. *IEEE Transactions on Antennas and Propagation*, 72 (1). pp. 962-967. ISSN 0018-926X.

## Downloaded from

<https://kar.kent.ac.uk/105016/> The University of Kent's Academic Repository KAR

## The version of record is available from

<https://doi.org/10.1109/TAP.2023.3329700>

## This document version

Author's Accepted Manuscript

## DOI for this version

## Licence for this version

CC BY (Attribution)

## Additional information

For the purpose of open access, the author has applied a CC BY public copyright licence to any Author Accepted Manuscript version arising from this submission.

## Versions of research works

### Versions of Record

If this version is the version of record, it is the same as the published version available on the publisher's web site. Cite as the published version.

### Author Accepted Manuscripts

If this document is identified as the Author Accepted Manuscript it is the version after peer review but before type setting, copy editing or publisher branding. Cite as Surname, Initial. (Year) 'Title of article'. To be published in **Title of Journal**, Volume and issue numbers [peer-reviewed accepted version]. Available at: DOI or URL (Accessed: date).

## Enquiries

If you have questions about this document contact [ResearchSupport@kent.ac.uk](mailto:ResearchSupport@kent.ac.uk). Please include the URL of the record in KAR. If you believe that your, or a third party's rights have been compromised through this document please see our [Take Down policy](https://www.kent.ac.uk/guides/kar-the-kent-academic-repository#policies) (available from <https://www.kent.ac.uk/guides/kar-the-kent-academic-repository#policies>).

# Wideband Dual-Polarized Antenna with High Selectivity for 5G Sub-6GHz Base Station Applications

Xuekang Liu, Benito Sanz-Izquierdo, Steven Gao, Haiwei Zhang, Wei Hu, Xue-Xia Yang and Josaphat Tetuko Sri Sumantyo

**Abstract**— A dual-polarized antenna with wide impedance bandwidth and high selectivity is presented for the use of 5G sub-6GHz base stations. By strategically introducing a novel coupled dual-mode grid structure, two additional resonant modes (One is in-band, another one is out-of-band) as well as two radiation nulls can be obtained to enhance the impedance bandwidth and out-of-band rejection level of the widely used tightly coupled cross-dipole antenna. The two radiation nulls introduced by the grid structure are located at the two edges of the desired frequency band. To further improve the gain suppression level in higher out-of-band, a new radiation null is obtained by symmetrically introducing four T-shaped strips. Apart from these additional radiation nulls, this antenna also exhibits two inherent radiation nulls originating from its feed structure and reflector. The measured results demonstrate that the proposed antenna exhibits a wide impedance bandwidth of 39.5% (ranging from 3.07 GHz to 4.58 GHz), excellent isolation of over 31 dB, and a notable out-of-band rejection level exceeding 17.6 dB and 19.2 dB in the frequency bands of 1.7 GHz-2.7 GHz and 4.8 GHz- 5.0 GHz.

**Index Terms**— Dual-polarized antenna, 5G sub-6GHz, high selectivity, base station.

## I. INTRODUCTION

As communication technology advances and the demand for high-quality connectivity increases, numerous countries around the world have declared their target frequency bands for 5G networks [1]. Compared to 5G mmWave bands, 5G sub-6GHz frequency bands strike a balance between coverage, capacity, penetration, and cost-effectiveness. Hence, during the initial phase of 5G technology development, these frequency bands have garnered significant attention. Several antenna designs have been proposed in [2]-[4] to cover one or multiple sub-6 GHz frequency bands for 5G. By using the vector synthesis technique, a dual-polarized antenna with high port isolation and low cross polarization is obtained in [2] to cover 3.3-3.6 GHz. The antenna in [3] can cover 3.17-3.77 GHz with a high isolation of 38.5 dB. However, its reference level of  $|S_{DD11}|$  is -10 dB, which is inconsistent with base station design requirements. Based on the cross magnetic dipoles [4], a  $\pm 45^\circ$  polarized antenna is realized to cover 3.38-5.1 GHz. However, these designs share a common drawback of insufficient out-of-band radiation suppression, a crucial aspect in the present-day design of base station antennas.

In modern base stations, there is a need to arrange numerous array antennas that operate across various frequency bands within a highly constrained space. However, this compact arrangement often results in significant mutual coupling among the antennas, which can degrade

This work was supported in part by Engineering and Physical Sciences Research Council (EPSRC) under Grant EP/S005625/1 and EP/N032497/1, and in part by Huawei Technologies Ltd. (Corresponding author: Xuekang Liu.)

Xuekang Liu and Benito Sanz-Izquierdo are with the School of Engineering, University of Kent, Canterbury CT2 7NT, U.K. (e-mail: [x1255@kent.ac.uk](mailto:x1255@kent.ac.uk)).

Steven Gao is with the Dept of Electronic Engineering, Chinese University of Hong Kong.

Haiwei Zhang is with the Huawei Technologies Ltd, China.

Wei Hu is with National Laboratory of Science and Technology on Antennas and Microwaves, Xidian University, Xi'an, Shaanxi 710071, China.

Xue-Xia Yang is with the School of Communication and Information Engineering, Shanghai University, Shanghai 200444, China.

Josaphat Tetuko Sri Sumantyo is with the Center for Environmental Remote Sensing, Chiba University, Chiba 263-8522, Japan.

their overall performance. By utilizing filtering antennas, the issue of cross-band mutual coupling can be effectively addressed. These antennas have the capability to transmit/receive signals within a specific frequency range while attenuating/rejecting signals that fall outside of that range [5]. This characteristic enables them to minimize the interference and coupling between different frequency bands, resulting in reduced mutual interference.

Several methods have been employed to achieve out-of-band rejection performance in various filtering antennas [6]-[24]. By replacing the last resonators of filters with radiators, two filtering antennas were presented in [6] and [7]. Stacked patch structure and slots are used in [9]-[13] to improve their selectivity. The profiles of these antennas are relatively low ( $<0.25 \lambda_0$ ). However, the impedance bandwidths of them are relatively narrow. The antennas in [16]-[19] were realized by using special feeding structures with filtering characteristics. A new method was proposed in [20] to introduce a radiation null in the design of filtering cross dipole antenna. When one of the dipoles is working, the dipole arms of its orthogonal counterpart act as parasitic resonators and can generate a radiation null without introducing other structure. With the help of the characteristic mode analysis, the antenna in [21] realized a measured -10 dB impedance bandwidth of 25% (3.3-4.25 GHz). However, the radiation pattern is not stable within the operating frequency band. The filtering antennas in [23] are realized by utilizing multiple folded dipoles and introducing parasitic structures. These designs effectively achieve a high level of out-of-band rejection performance.

Tightly coupled cross-dipole antenna (TCCDA) [25],[26] is widely used in base station applications due to its stable radiation patterns, high gain, and good impedance bandwidth. Nevertheless, there is a need to enhance the out-of-band suppression ability of them in order to meet the demand for low cross-band mutual coupling in modern, highly integrated systems. A filtering TCCDA was realized in [27] by introducing parasitic loop and open stub. This antenna has a good gain suppression level in lower frequency band. However, it lacks the ability to suppress the radiation of higher frequency band.

In this communication, a dual-polarized filtering antenna with broad impedance bandwidth and high out-of-band gain suppression level in both lower and higher frequency bands is presented based on the TCCDA. A dual-mode grid structure is used in this research to generate two resonant modes and two radiation nulls. Besides, by incorporating four T-shaped strips, an additional radiation null is introduced, further improving the gain suppression level of the antenna. Furthermore, two inherent radiation nulls are analyzed and adjusted to enhance the selectivity of the proposed antenna. The proposed antenna presents a considerable advancement over the commonly used TCCDA with similar specifications in terms of impedance bandwidth and selectivity. These enhancements make it has a good application prospect in the base station applications.

## II. CONFIGURATION AND WORKING PRINCIPLE

### A. Antenna Configuration and Comparison

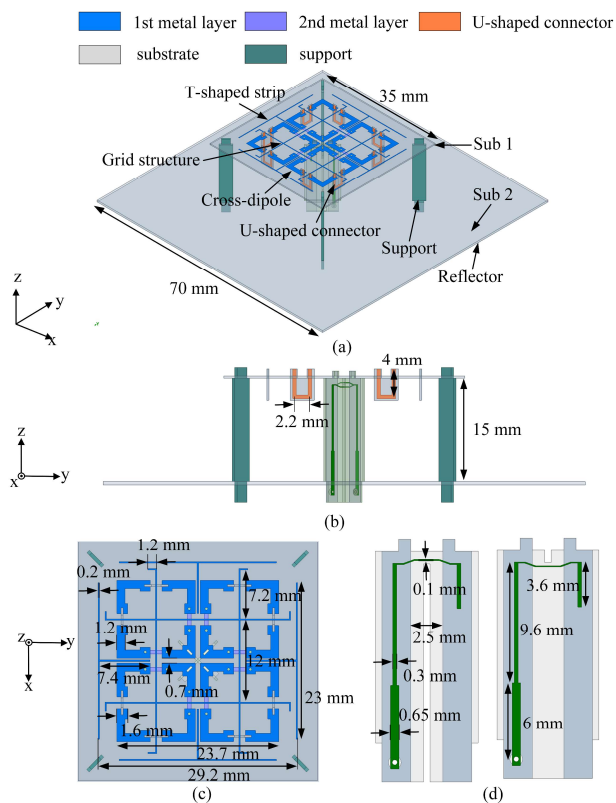


Fig. 1. Configuration of the proposed antenna. (a) 3D view, (b) side view, (c) top view, and (d) balun.

Fig.1 shows the configuration of the proposed dual-polarized filtering antenna. This antenna contains four parts: the feeding balun [28], the support structure, the reflector, and the radiator which consists of the cross-dipole, the U-shaped connectors, the grid structure, and the T-shaped strips. In this design, all the metal structures are printed on Rogers 4003 substrates with a relative dielectric permittivity of 3.55. The thickness of the substrate with reflector is 0.508mm. The thickness of other substrates is 0.305 mm. The T-shaped strips, grid structure, and the majority of the cross-dipole are printed on the upper layer of substrate 1. To prevent intersection with the grid structure, a section of the cross-dipole is printed on the lower layer of substrate 1. The U-shaped connectors are vertically connected to the cross-dipole to reduce the aperture of the cross-dipole. The radiator and the reflector are connected by the feeding baluns. All the detailed dimensions are given in millimeters in Fig. 1(a), (b), (c), and (d).

To better showcase the superiority of this design, a common tightly coupled cross-dipole antenna (TCCDA) was also designed with the same profile. The configuration of the TCCDA is illustrated in Fig.2 (a) and (b). It is a conventional cross-dipole antenna widely used in nowadays base stations. Notably, the aperture of the TCCDA measures 30.8 mm × 30.8 mm, which is larger than the proposed antenna's aperture of 29.2 mm × 29.2 mm. The simulated  $|S_{11}|$  and normalized peak realized gain of the proposed antenna and TCCDA are shown in Fig. 2(c). As can be seen, the proposed antenna exhibits a significantly broader impedance bandwidth compared to the TCCDA with identical specifications. Furthermore, the proposed antenna demonstrates superior out-of-band gain suppression level, featuring additional radiation nulls and a steeper roll-off rate when compared to the TCCDA. It can be observed that the proposed antenna

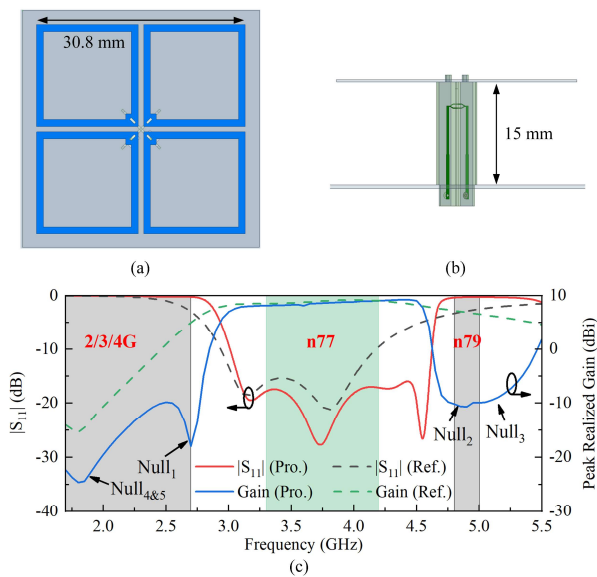


Fig. 2. (a) Top view of the TCCDA, (b) side view of the TCCDA, and (c) simulated  $|S_{11}|$  and gain of the TCCDA and proposed antenna.

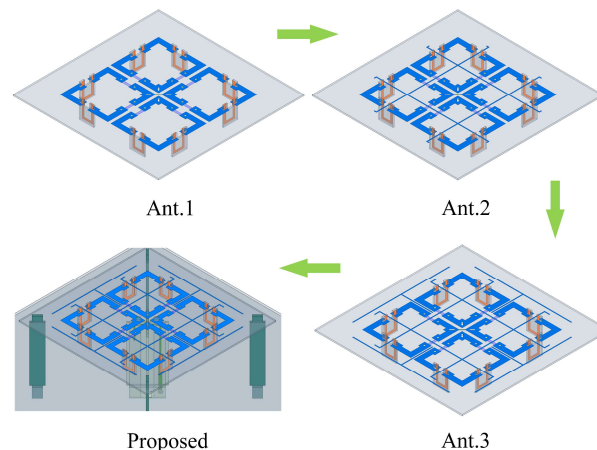


Fig. 3. Evolution of the proposed antenna.

can cover the entire n77 band (3.3-4.2 GHz) while maintaining a high level of out-of-band suppression in the 2/3/4G frequency bands (1.7-2.7 GHz) and the n79 band (4.8-5.0 GHz). This exceptional performance aligns well with the requirements of modern 5G base station designs.

To better illustrate the working principle of the four radiation nulls, three reference antennas were simulated and analyzed. As depicted in Fig. 3, none of the reference antennas (Ant.1, Ant.2, and Ant.3) contain reflectors and are all fed by ideally lumped ports. Ant.1 is a TCCDA with modified arms. By introducing the U-shaped connectors on dipole arms, the aperture of the TCCDA can be effectively reduced. Then, by introducing the parasitic grid structure, two radiation nulls can be obtained in Ant.2 at lower (1<sup>st</sup> radiation null) and higher (2<sup>nd</sup> radiation null) frequency bands. To further enhance gain rejection level of the higher out-of-band, four T-shaped strips are printed around the cross-dipole in Ant.3. These T-shaped strips can introduce a new radiation null (3<sup>rd</sup> radiation null) next to the existing higher-band radiation null (2<sup>nd</sup> radiation null). Finally, two baluns are used to feed the cross-dipole with balanced signal. An inherent radiation null (4<sup>th</sup> radiation null) can also be excited after introducing these feed

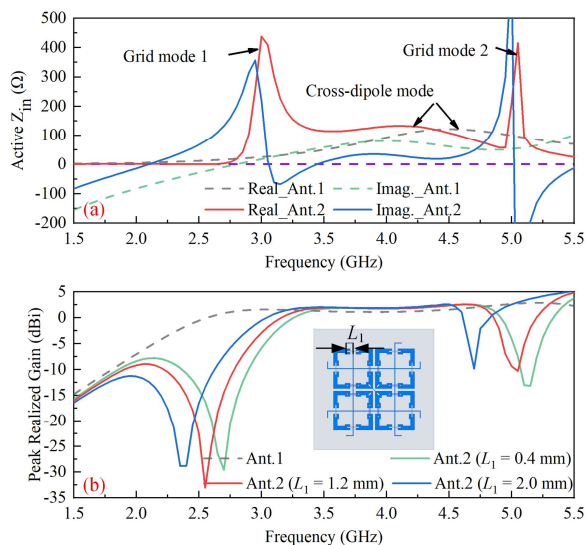


Fig. 4. Simulated (a) input impedances and (b) peak realized gains of the reference Ant.1 and Ant.2.

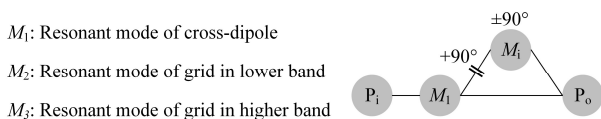


Fig. 5. Multipath coupling diagram for grid mode 1 and 2.

structure. A reflector is used to optimize the radiation pattern of the proposed antenna and introduce another inherent radiation ( $5^{\text{th}}$  radiation null). The working principles of the radiation nulls will be explained in the following sections.

### B. The 1<sup>st</sup> and 2<sup>nd</sup> Radiation Nulls

The multipath coupling method [29] is a good choice for designing a filtering antenna due to its inherent advantages of easy implementation and controllability. In multipath coupling diagram, each resonator can be seen as a parallel  $RLC$  combination. The coupling between these resonators can be represented by inductors ( $-90^\circ$  phase shift) and capacitors ( $+90^\circ$  phase shift). When the multipath coupling amplitude from the source to the load is equal but the phase is opposite, the transmission zero point can be obtained. In this design, the tightly coupled cross-dipole is connected to the baluns directly. Thus, it can be seen as the main path from the source to the load. In this case, new radiation nulls can be obtained to form a wideband filtering antenna by reasonably adjust the coupling method between the cross-dipole and parasitic resonators to achieve phase inversion.

The simulated input impedances and peak realized gains of the reference Ant.1 and Ant.2 are shown in Fig. 4. Different from other parasitic structures, the grid structure in this design has two different working modes. Thus, two radiation nulls can be provided when these working modes are reasonably excited. As can be seen in Fig.4, two new resonant modes and two radiation nulls can be obtained after introducing the parasitic grid structure. The input resistance of the Ant.1 varies from  $40 \Omega$  to  $125 \Omega$  within the frequency range of 3.2-4.5 GHz. Meanwhile, the input reactance of Ant.1 remains consistently around  $60 \Omega$ . It is obvious that Ant.1, with such unstable input impedance, poses significant challenges for achieving a proper match, especially when adhering to a stringent reference level of  $|S_{11}| < -14$  dB, using baluns. However, with the introduction of the grid

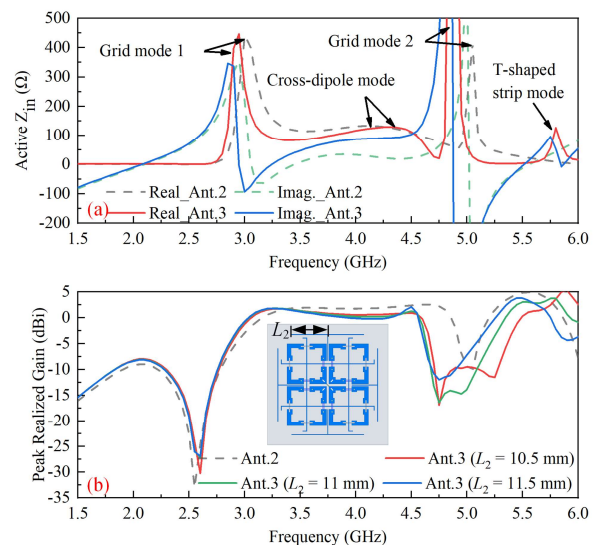


Fig. 6. Simulated (a) input impedances and (b) peak realized gains of the reference Ant.2 and Ant.3.

structure, the input resistance of Ant. 2 is consistently maintained at approximately  $125 \Omega$  within the 3.2-4.5 GHz range, and its input reactance remains close to  $0 \Omega$ . This makes it considerably easier to achieve a good impedance matching.

The multipath coupling diagram of the proposed antenna near these two resonant modes are given in Fig. 5.  $P_i$  and  $P_o$  are input and output ports of the antenna, respectively.  $M_1$ ,  $M_2$ , and  $M_3$  represent the resonant mode of the cross-dipole, the grid in lower band and higher band. The electric coupling between the cross-dipole and the parasitic grid is expressed as a capacitor. Depending on the frequency of interest, the coupled resonators provide phase shifts of  $+90^\circ$  and  $-90^\circ$ . Specifically, below the resonant frequency of the coupled resonator, the phase shift is  $+90^\circ$ , while above the resonant frequency, it becomes  $-90^\circ$ . Assuming a total phase shift of  $0^\circ$  for the main path ( $P_i$ - $M_1$ - $P_o$ ) [30], transmission zeros can be achieved by attaining a total phase shift of  $180^\circ$  in the parasitic path. Considering the  $+90^\circ$  phase shift of the electric coupling, it can be concluded that radiation nulls can be realized below the resonant frequencies of the coupled resonators.

The relationship between the frequencies of the radiation nulls and the length of the grid ( $L_1$ ) is shown in Fig. 4(b). Both radiation nulls shift toward lower frequency bands when the  $L_1$  increase. Moreover, the frequency ratio of the two radiation nulls is almost constant at 2:1 during the change of  $L_1$ .

### C. The 3<sup>rd</sup> Radiation Null

To further enhance the gain suppression level of the proposed antenna in higher out-of-band. The 3<sup>rd</sup> radiation null is introduced by placing four T-shaped strips around the cross-dipole. As can be seen in Fig. 6, a new resonant mode (resonant mode of T-shaped strips) is excited at 5.8 GHz. Although this resonant mode cannot be used to enhance the bandwidth of the proposed antenna. It can introduce a radiation null below its resonant frequency according to the analysis in sub-section B. As shown in Fig. 6(b), the 3<sup>rd</sup> radiation null appears at 5.25 GHz. And the gain suppression level in higher out-of-band can be successfully improved by the new radiation null. The multipath coupling diagram for this resonant mode is like the grid modes, thus no duplicate analysis is performed in this sub-section. The relationship between the frequency of the 3<sup>rd</sup> radiation null and  $L_2$  is given in Fig. 6(b). When  $L_2$  increase from 10.5 mm to 11.5 mm, the 3<sup>rd</sup> radiation

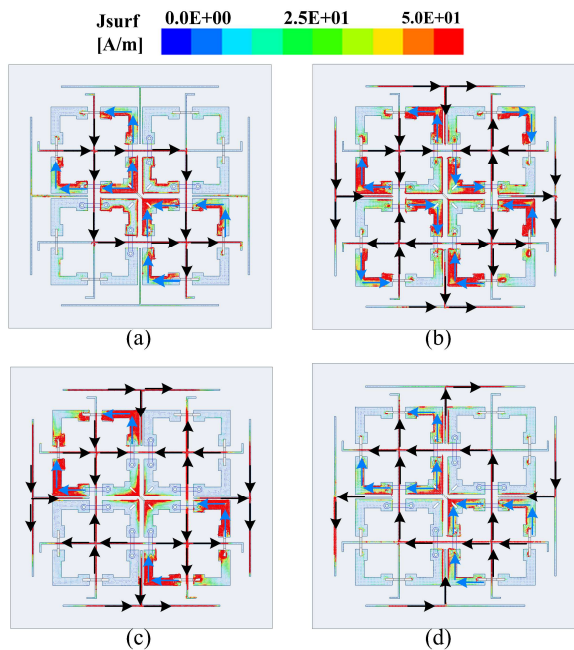


Fig. 7. Simulated current distributions on Ant.3 at (a) 2.6 GHz (out-of-band), (b) 4.75 GHz (out-of-band), (c) 5.25 GHz (out-of-band), and (d) 3.5 GHz (in-band).

null shifts from 5.25 GHz to 4.85 GHz without influencing other radiation nulls.

The current distributions on Ant.3 at different frequencies are shown in Fig. 7. As illustrated in Fig. 7(a), the maximum current density is observed on the dipole arms and grid structure, with the current vectors on these components being in opposing directions (out-of-phase) at 2.6 GHz (out-of-band). Similarly, at 4.75 GHz (out-of-band) and 5.25 GHz (out-of-band), the current vectors on the grid structure and T-shaped strips are also opposite to the current vectors on the dipole arms. These provide further evidence supporting the existence of radiation nulls at these frequencies from an alternative perspective. However, at 3.5 GHz (in-band), the current vectors align in the same direction on the dipole arms, the grid structure, and a portion of the T-shaped strips, leading to radiation.

### C. The 4<sup>th</sup> and 5<sup>th</sup> Radiation Null

The 4<sup>th</sup> and 5<sup>th</sup> radiation nulls in this design are superimposed, so they are not clearly distinguishable from the simulated gain. They can be separated by adjusting the reflector size, as shown in Fig. 8. The 4<sup>th</sup> radiation null in this design is caused by the  $\frac{1}{4} \lambda_g$  resonant mode of the dipole arm and feeding baluns mentioned in [31]. The size of the reflector has little influence on the frequency of this radiation null. The working principle of this radiation null has been analyzed in [31].

The 5<sup>th</sup> radiation null is introduced by the reflector. The size of the reflector has large effect on the frequency of this radiation null. For the incident waves, the reflector can be seen as surface impedance  $Z_s$  ( $Z_s \approx 0$  for PEC,  $Z_s \approx \infty$  for PMC). In this design, since the reflector is finite copper conductor, which resonates at a certain frequency ( $1/2 \lambda_g$  resonant mode), it can be seen as a series  $RLC$  circuit [32] with a low  $R$ . When it resonates, the incident waves will be reflected with a  $180^\circ$  phase shift. Taking the distance between the antenna and reflector into consideration ( $< 1/10 \lambda_f$ ,  $\lambda_f$  is the wavelength at the resonant frequency of the reflector), a radiation null can be obtained.

The relationship between the frequency of the 5<sup>th</sup> radiation null and the size of the reflector is shown in Fig.8. As can be observed, the 5<sup>th</sup>

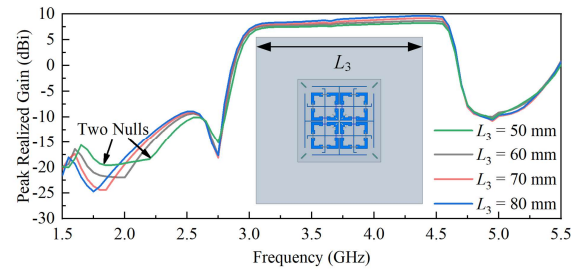


Fig. 8. Simulated peak realized gains of the proposed antenna with different  $L_3$ .

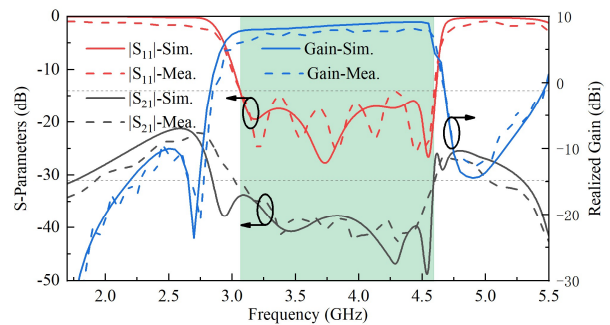


Fig. 9. Measured and simulated  $|S_{11}|$ ,  $|S_{21}|$ , and realized gain at boresight direction.

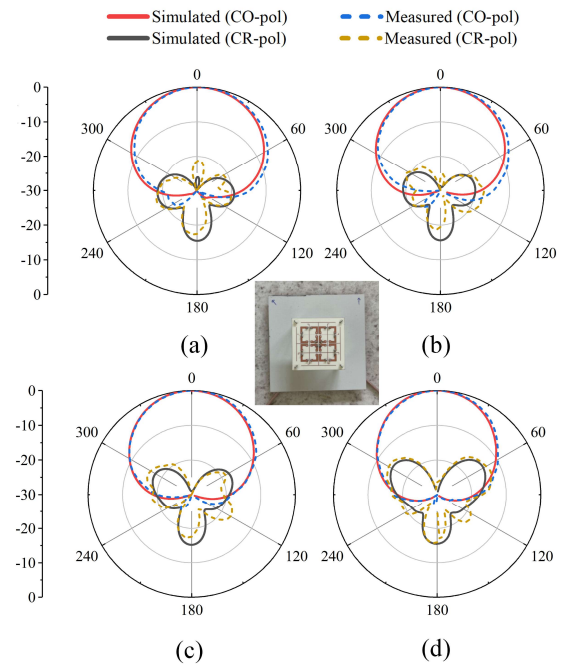


Fig. 10. Normalized radiation patterns in horizontal plane of the proposed antenna at (a) 3.2 GHz, (b) 3.6 GHz, (c) 4.0 GHz, and (d) 4.4 GHz.

radiation null shifts from 2.25 GHz to 1.75 GHz when the size of the reflector increase from 50 mm to 80 mm. Furthermore, alterations in the dimensions of the reflector have little effect on other radiation nulls.

### III. MEASURED RESULTS OF THE ELEMENT

A prototype of the proposed antenna element was fabricated and tested. The measured S-parameters were obtained by using the Keysight P9377B VNA in antenna lab at the University of Kent. From

TABLE I  
COMPARISON WITH OTHER 5G SUB-6GHZ ANTENNAS

Ref.	Polar.	BW	Size ( $\lambda_0^3$ )	Gain (dBi)	Nulls	Rej. (dB)
[4]	$\pm 45^\circ$	3.38-5.20 (42.4%)	$0.61 \times 0.61 \times 0.25$	7	/	/
[11]	Single	3.16-3.84 *(19.4%)	$0.39 \times 0.36 \times 0.08$	8.55	2	20.7; 19.2
[12]	$\pm 90^\circ$	3.19-3.85 *(18%)	$0.75 \times 0.75 \times 0.09$	9.5	2	12.9; /
[13]	$\pm 90^\circ$	3.15-4.25 *(29.7%)	$0.61 \times 0.61 \times 0.09$	9.5	2	16; 13
[19]	Single	3.28-3.80 *(14%)	$0.54 \times 0.54 \times 0.08$	7.5	3	19.1; 23.6
[27]	$\pm 45^\circ$	3.30-3.80 (14%)	$0.34 \times 0.34 \times 0.21$	7.4	2	17; /
<b>Pro. TCCDA</b>	<b><math>\pm 45^\circ</math></b>	<b>3.07-4.58 (39.5%)</b>	<b><math>0.37 \times 0.37 \times 0.20</math></b>	<b>8.1</b>	<b>5</b>	<b>17.6; 19.2</b>

\* means the reference level of  $|S_{11}|$  is -10 dB. Polar. represents polarization. Rej. Represents rejection level in 1.7-2.7 GHz and 4.8-5.0 GHz.

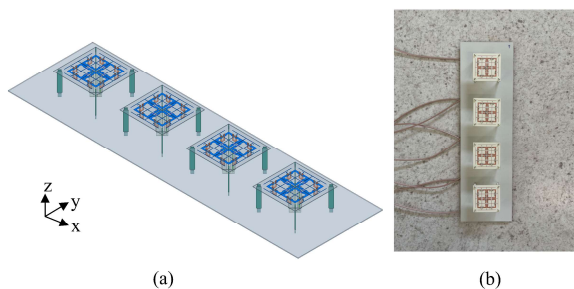


Fig. 11. (a) Configuration of the four element array antenna, and (b) photo of the fabricated antenna.

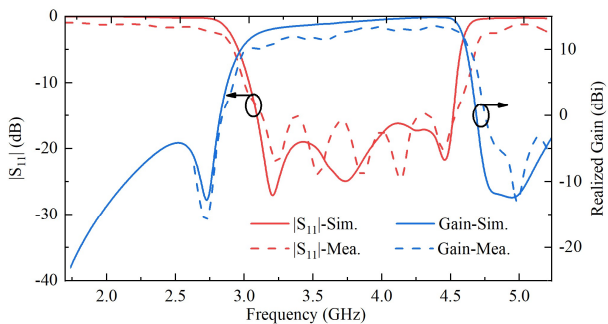


Fig. 12. Measured and simulated  $|S_{11}|$  and realized gain at boresight direction.

the measured results in Fig. 9, it can be observed that the measured -14 dB impedance bandwidth is 39.5% (from 3.07 GHz to 4.58 GHz), which is consistent with the simulated result. The isolation between the two polarizations is higher than 31 dB within the working frequency band.

The far-field performance of the proposed antenna was measured in the anechoic chamber. As given in Fig. 9, the proposed antenna achieves a peak measured gain of 8.1 dBi. It is worth noting that this value is slightly lower than the simulated gain of 9.1 dBi. This difference can be attributed to the measurement errors, and the insertion loss of the cables used in the experiment. Besides, the proposed antenna realizes a good out-of-band rejection level of more than 17.6 dB and 19.2 dB in 1.7 GHz -2.7 GHz, and 4.8 GHz- 5.0 GHz bands. The comparison between the measured and simulated radiation

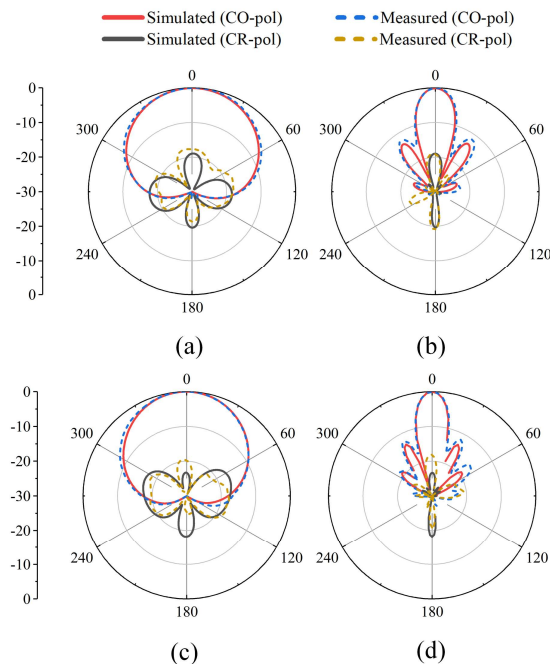


Fig. 13. Normalized radiation patterns in horizontal (a) and (c) and vertical (b) and (d) plane of the proposed antenna at 3.4 GHz and 4.2 GHz.

patterns at different frequencies are given in Fig. 10. Due to the symmetry of the antenna, only the patterns in the horizontal plane are given. The measured radiation patterns agree well with the simulated results. The half-power beamwidth of the proposed antenna in horizontal plane is  $67.5^\circ \pm 6.5^\circ$ . The cross-polarization level is 21 dB lower than the co-polarization level at boresight direction. Besides, the radiation patterns of the antenna is very stable within the operating frequency bands.

The  $\pm 45^\circ$  polarized antenna in [4] realizes a wider impedance bandwidth than the proposed antenna at the expense of increased size. However, the lack of filtering characteristics prevents it from reducing cross-band interference. Two filtering antennas cover n78 band with good out-of-band rejection level were presented in [11] and [19]. However, their single polarization characteristics make them unsuitable for nowadays base station applications. The  $\pm 90^\circ$  polarized filtering antennas in [12] and [13] can cover n78 and n77 bands, respectively. Since the aperture of these antennas are relatively large, a better peak realized gain of 9.5 dBi was realized. However, the out-of-band rejection levels of them are lower than the proposed design. Besides, the reference level of reflection coefficient of them is -10 dB, rather than -14 dB. A similar  $\pm 45^\circ$  polarized filtering antenna based on the TCCDA was developed in [27] for 5G sub-6GHz base station applications. Compared with this design, the proposed antenna achieves a wider impedance bandwidth, higher peak realized gain, more radiation nulls and better out-of-band suppression characteristics under the similar size.

#### IV. FOUR ELEMENT ARRAY

To explore the performance of the proposed antenna in array configuration, a four element array antenna was designed, simulated, fabricated, and measured. The configuration of the proposed array antenna is shown in Fig. 11(a). The reflector is with a size of 240 mm  $\times$  70 mm. The distance between the antenna elements is 55 mm, which is  $0.56 \lambda_{3.07\text{GHz}}$  and  $0.84 \lambda_{4.58\text{GHz}}$ . The configuration of the antenna element in the array are consistent with the one in Fig. 1.

To validate the design principle, a prototype of the array antenna was also fabricated, as display in Fig. 11(b). The measured and simulated reflection coefficient and realized gain at boresight direction of the array is given in Fig. 12. The measured results demonstrate that the array antenna has an impedance bandwidth of 37.5% (3.12 GHz – 4.56 GHz). The measured peak realized gain is 13.7 dBi within the operating frequency band. Fig. 13 shows the measured and simulated normalized radiation patterns of the proposed antenna in horizontal and vertical planes. The half power beamwidths of the proposed array antenna are  $72^\circ$  and  $20^\circ$  in horizontal and vertical plane at 3.4 GHz, respectively. At 4.2 GHz, the half power beamwidths of the proposed array antenna are  $64^\circ$  and  $16^\circ$  in horizontal and vertical plane.

#### V. CONCLUSION

A novel dual-polarized filtering antenna with wide impedance bandwidth and high out-of-band rejection level is proposed in this communication. All the radiation nulls can be individually tuned without affecting other radiation nulls by adjusting their corresponding structures. In comparison to the widely used TCCDA with similar specifications, the proposed antenna demonstrates a considerably wider impedance bandwidth and a notably improved selectivity, which are crucial characteristics in modern base station antenna designs. To validate the design concept, both a single antenna element and a four-element array antenna were fabricated and tested. The measured results closely align with the simulated results, confirming the outstanding performance of this antenna. Such exceptional performance instills a high level of confidence in its potential application in base station systems.

#### REFERENCES

- [1] Global update on spectrum for 4G & 5G. Accessed: Dec. 2020. [online]. Available: [https://www.qualcomm.com/content/dam/qcomm-martech/dm-assets/documents/messaging\\_presentation\\_-\\_4g\\_5g\\_spectrums\\_-\\_december\\_2020.pdf](https://www.qualcomm.com/content/dam/qcomm-martech/dm-assets/documents/messaging_presentation_-_4g_5g_spectrums_-_december_2020.pdf).
- [2] H. Huang, X. Li and Y. Liu, "5G MIMO antenna based on vector synthetic mechanism," *IEEE Antennas Wireless Propag. Lett.*, vol. 17, no. 6, pp. 1052-1055, June 2018.
- [3] L. -H. Wen, S. Gao, Q. Luo, Q. Yang, W. Hu and Y. Yin, "A low-cost differentially driven dual-polarized patch antenna by using open-loop resonators," *IEEE Trans. Antennas Propag.*, vol. 67, no. 4, pp. 2745-2750, April 2019.
- [4] Y. Qin, L. Zhang, C. -X. Mao and H. Zhu, "A compact wideband Antenna with suppressed mutual coupling for 5G MIMO applications," *IEEE Antennas Wireless Propag. Lett.*, vol. 22, no. 4, pp. 938-942, April 2023.
- [5] G. Q. Luo et al., "Filtenna consisting of horn antenna and substrate integrated waveguide cavity FSS," *IEEE Trans. Antennas Propag.*, vol. 55, no. 1, pp. 92-98, Jan 2007.
- [6] W. -J. Wu, Y. -Z. Yin, S. -L. Zuo, Z. -Y. Zhang and J. -J. Xie, "A new compact filter-antenna for modern wireless communication systems," *IEEE Antennas Wireless Propag. Lett.*, vol. 10, pp. 1131-1134, 2011.
- [7] C. -T. Chuang and S. -J. Chung, "Synthesis and design of a new printed filtering antenna," *IEEE Trans. Antennas Propag.*, vol. 59, no. 3, pp. 1036-1042, March 2011.
- [8] X. Liu et al., "A compact dual-polarized filtering antenna with steep cut-off for base-station applications," *IEEE Trans. Antennas Propag.*, vol. 70, no. 7, pp. 5941-5946, July 2022.
- [9] X. Y. Zhang, W. Duan and Y. -M. Pan, "High-gain filtering patch antenna without extra circuit," *IEEE Trans. Antennas Propag.*, vol. 63, no. 12, pp. 5883-5888, Dec 2015.
- [10] K. Xue, D. Yang, C. Guo, H. Zhai, H. Li and Y. Zeng, "A dual-polarized filtering base-station antenna with compact size for 5G applications," *IEEE Antennas Wireless Propag. Lett.*, vol. 19, no. 8, pp. 1316-1320, Aug. 2020.
- [11] S. Liu, Z. Wang and Y. Dong, "A compact coupling-fed patch antenna with quasi-elliptical filtering response," *IEEE Antennas Wireless Propag. Lett.*, doi: 10.1109/LAWP.2023.3311989.
- [12] H. Yuan, F. -C. Chen and Q. -X. Chu, "A wideband and high gain dual-polarized filtering antenna based on multiple patches," *IEEE Trans. Antennas Propag.*, vol. 70, no. 10, pp. 9843-9848, Oct. 2022.
- [13] Y. Q. Sun, Z. J. Zhai, D. H. Zhao, F. Lin, X. Y. Zhang and H. J. Sun, "High-gain low cross-polarized dual-polarized filtering patch antenna without extra circuits," *IEEE Antennas Wireless Propag. Lett.*, vol. 21, no. 7, pp. 1368-1372, July 2022.
- [14] J. W. Wang, R. Ma, S. F. Bo, H. Huang and X. Y. Zhang, "Multipath-coupling based filtenna for base-station applications," *IEEE Trans. Antennas Propag.*, doi: 10.1109/TAP.2023.3306466.
- [15] T. Wang, N. Yan, M. Tian, Y. Luo and K. Ma, "A low-cost high-gain filtering patch antenna with enhanced frequency selectivity based on SISL for 5G application," *IEEE Antennas Wireless Propag. Lett.*, vol. 21, no. 9, pp. 1772-1776, Sept. 2022.
- [16] D. Yang, H. Zhai, C. Guo and C. Ma, "A novel differentially fed dual-polarized filtering magneto-electric dipole antenna for 5G base station applications," *IEEE Trans. Antennas Propag.*, vol. 70, no. 7, pp. 5373-5382, July 2022.
- [17] S. J. Yang, Y. M. Pan, Y. Zhang, Y. Gao and X. Y. Zhang, "Low-profile dual-polarized filtering magneto-electric dipole antenna for 5G applications," *IEEE Trans. Antennas Propag.*, vol. 67, no. 10, pp. 6235-6243, Oct. 2019.
- [18] Y. Liu, S. Wang, N. Li, J. -B. Wang and J. Zhao, "A compact dual-band dual-polarized antenna with filtering structures for sub-6 GHz base station applications," *IEEE Antennas Wireless Propag. Lett.*, vol. 17, no. 10, pp. 1764-1768, Oct. 2018.
- [19] Z. -T. Du, K. X. Wang, Z. Chen and H. Wong, "Design of a filtering antenna with hybrid feed structure for 5G communications," *IEEE Trans. Antennas Propag.*, doi: 10.1109/TAP.2023.3312922.
- [20] X. Liu, B. Sanz-Izquierdo, H. Zhang and S. Gao, "A wideband dual-polarized filtering antenna for multi-band base station application," in *Proc. 17th Eur. Conf. Antennas Propag.*, 2023, pp. 1-5.
- [21] J. Guo, Y. Chen, D. Yang, B. Ma, S. Liu and J. Pan, "Design of a circuit-free filtering metasurface antenna using characteristic mode analysis," *IEEE Trans. Antennas Propag.*, vol. 70, no. 12, pp. 12322-12327, Dec. 2022.
- [22] B. -J. Chen and X. -S. Yang, "Compact dual-polarized filtering antenna based on differential feeding and double-layer metasurface," *IEEE Trans. Antennas Propag.*, vol. 71, no. 1, pp. 1065-1070, Jan. 2023.
- [23] X. Liu et al., "A mutual-coupling-suppressed dual-band dual-polarized base station antenna using multiple folded-dipole antenna," *IEEE Trans. Antennas Propag.*, vol. 70, no. 12, pp. 11582-11594, Dec. 2022.
- [24] R. Hou, J. Ren, Y. -T. Liu, Y. -M. Cai, J. Wang and Y. Yin, "Broadband magnetolectric dipole filtering antenna for 5G application," *IEEE Antennas Wireless Propag. Lett.*, vol. 22, no. 3, pp. 497-501, March 2023.
- [25] Z. Bao, Z. Nie and X. Zong, "A novel broadband dual-polarization antenna utilizing strong mutual coupling," *IEEE Trans. Antennas Propag.*, vol. 62, no. 1, pp. 450-454, Jan. 2014.
- [26] C. Ding, H. Sun, R. W. Ziolkowski and Y. J. Guo, "Simplified tightly coupled cross-dipole arrangement for base station applications," *IEEE Access.*, vol. 5, pp. 27491-27503, 2017.
- [27] S. J. Yang, W. Duan, Y. Y. Liu, H. Ye, H. Yang and X. Y. Zhang, "Compact dual-band base-station antenna using filtering elements," *IEEE Trans. Antennas Propag.*, vol. 70, no. 8, pp. 7106-7111, Aug. 2022.
- [28] R. Li, T. Wu, B. Pan, K. Lim, J. Laskar and M. M. Tentzeris, "Equivalent-circuit analysis of a broadband printed dipole with adjusted integrated balun and an array for base station applications," *IEEE Trans. Antennas Propag.*, vol. 57, no. 7, pp. 2180-2184, July. 2009.
- [29] J. B. Thomas, "Cross-coupling in coaxial cavity filters - a tutorial overview," *IEEE Trans. Microw. Theory Techn.*, vol. 51, no. 4, pp. 1368-1376, April 2003.
- [30] J. -F. Qian, F. -C. Chen, Q. -X. Chu, Q. Xue and M. J. Lancaster, "A novel electric and magnetic gap-coupled broadband patch antenna with improved selectivity and its application in MIMO system," *IEEE Trans. Antennas Propag.*, vol. 66, no. 10, pp. 5625-5629, Oct. 2018.
- [31] Y. F. Cao, Y. F. Wu, Y. -M. Pan and X. Y. Zhang, "A Method of Generating Radiation Nulls Utilizing Inherent Resonance Modes for Dual-Polarized Filtering Dipole Antenna Design," *IEEE Trans. Antennas Propag.*, vol. 68, no. 8, pp. 6413-6418, Aug. 2020.
- [32] L. Peng, J. Xie, K. Sun, X. Jiang, and S. Li, "Resonance-based reflector and its application in unidirectional antenna with low-profile and broadband characteristics for wireless applications," *Sensors.*, vol. 16, no. 12, p. 2092, Dec. 2016.